

In vivo single-shot ^{13}C spectroscopic imaging of hyperpolarized metabolites by spatiotemporal encoding



Rita Schmidt^a, Christoffer Laustsen^{b,c}, Jean-Nicolas Dumez^a, Mikko I. Kettunen^{d,e}, Eva M. Serrao^{d,e}, Irene Marco-Rius^{d,e}, Kevin M. Brindle^{d,e}, Jan Henrik Ardenkjaer-Larsen^{c,f}, Lucio Frydman^{a,*}

^a Department of Chemical Physics, Weizmann Institute of Science, Rehovot, Israel

^b MR Research Centre, Aarhus University, Denmark

^c Danish Research Centre for Magnetic Resonance, Hvidovre Hospital, Denmark

^d Department of Biochemistry, University of Cambridge, Cambridge, United Kingdom

^e Cancer Research UK Cambridge Institute, Li Ka Shing Centre, Cambridge, United Kingdom

^f GE Healthcare, Broendby, Denmark

ARTICLE INFO

Article history:

Received 12 September 2013

Revised 17 November 2013

Available online 12 January 2014

Keywords:

Ultrafast MRI

Chemical shift imaging

Spatiotemporal encoding

Hyperpolarized dynamic imaging

Hyperpolarized MRI

DNP

Spectroscopic imaging

Cancer

ABSTRACT

Hyperpolarized metabolic imaging is a growing field that has provided a new tool for analyzing metabolism, particularly in cancer. Given the short life times of the hyperpolarized signal, fast and effective spectroscopic imaging methods compatible with dynamic metabolic characterizations are necessary. Several approaches have been customized for hyperpolarized ^{13}C MRI, including CSI with a center-out k -space encoding, EPSI, and spectrally selective pulses in combination with spiral EPI acquisitions. Recent studies have described the potential of single-shot alternatives based on spatiotemporal encoding (SPEN) principles, to derive chemical-shift images within a sub-second period. By contrast to EPSI, SPEN does not require oscillating acquisition gradients to deliver chemical-shift information: its signal encodes both spatial as well as chemical shift information, at no extra cost in experimental complexity. SPEN MRI sequences with slice-selection and arbitrary excitation pulses can also be devised, endowing SPEN with the potential to deliver single-shot multi-slice chemical shift images, with a temporal resolution required for hyperpolarized dynamic metabolic imaging. The present work demonstrates this with initial *in vivo* results obtained from SPEN-based imaging of pyruvate and its metabolic products, after injection of hyperpolarized $[1-^{13}\text{C}]$ pyruvate. Multi-slice chemical-shift images of healthy rats were obtained at 4.7 T in the region of the kidney, and 4D (2D spatial, 1D spectral, 1D temporal) data sets were obtained at 7 T from a murine lymphoma tumor model.

© 2014 Elsevier Inc. All rights reserved.

1. Introduction

The importance of Magnetic Resonance Spectroscopic Imaging (MRSI) in preclinical and clinical studies has been enhanced by the emergence of dissolution dynamic nuclear polarization (d-DNP). Dissolution DNP has opened new horizons in dynamic metabolic imaging through ^{13}C spectral observations of hyperpolarized compounds *in vivo* [1,2]. DNP can result in signal enhancements >10,000 for ^{13}C ; an unprecedented increase that is leading to

Abbreviations: CSI, chemical shift imaging; EPI, echo-planar imaging; EPSI, echo-planar spectroscopic imaging; d-DNP, dissolution dynamic nuclear polarization; FOV, field of view; FT, Fourier Transform; MRI, Magnetic Resonance Imaging; NMR, Nuclear Magnetic Resonance; PE, Phase Encode; RF, Radio frequency; RO, Read Out; SAR, Specific Absorption Rate; SPEN, SPatiotemporal ENcoding; SR, super resolution; TE, Echo Time.

* Corresponding author.

E-mail address: Lucio.frydman@weizmann.ac.il (L. Frydman).

new opportunities for imaging pathology and monitoring treatment [3–7]. Pyruvic acid has emerged as the principal ^{13}C -labeled agent in d-DNP, but there is significant on-going research to develop other compounds for dynamic imaging of metabolism [8–10]. Despite this unique potential, *in vivo* d-DNP ^{13}C NMR remains a challenge. The hyperpolarization decays irreversibly with T_1 , as well as following the spins' excitation. Thus fast schemes, capable of delivering both spatial and spectral information from these transient signals, are required to exploit the opportunities opened by these experiments. A variety of strategies have been developed to deal with these demanding requirements; including multi-band pulses [11], variable-flip-angle excitations with pulse angles optimized for the injected hyperpolarized species and their products [12], spiral and blipped echo-planar imaging (EPI) acquisitions [13], and compressed sensing strategies [14]. Principal among the strategies in current d-DNP use are multi-scan chemical shift imaging (CSI) or IDEAL type sequences

with a center-out phase-encoding scheme [15,16], and echo-planar spectroscopic imaging (EPSI) modules [17]. Both of these acquisition modes can provide practical spatial and spectral resolutions, albeit in multiple scans. EPI with suitable scan parameters can also be used for simultaneous imaging of two chemical shifts [18]. Each of these excitation and acquisition schemes makes some tradeoff in spatial, spectral and temporal resolution, and the most suitable approach depends on the application.

An alternative approach to single-shot imaging, which departs from traditional k -space concepts, has been developed over the last few years. First introduced for the acquisition of 2D NMR spectra in a single scan [19,20], spatiotemporal encoding (SPEN) utilizes a chirped pulse combined with a gradient for a sequential manipulation of the spins that can directly monitor their density in real space [21,22]. In an imaging context, SPEN uses such a manipulation along the low-bandwidth domain in combination with a conventional k -space readout, leading to a so-called hybrid acquisition mode [23,24]. Hybrid SPEN has a higher robustness against magnetic field inhomogeneities than EPI, reflecting the larger bandwidths it can access for the spatially sequential excitation and detection. This is aided by the possibility of refocusing all of the spin packets throughout acquisition [25,26]. Equally important is the fact that SPEN allows spectral-spatial imaging, at no additional expense over the basic imaging pulse sequence [27]. Further refinements arise from the use of super resolution (SR) and of other reconstruction methods to improve SPEN images by extracting the overlapping information included in the measured data points [28,29]. SR algorithms have also been extended to include chemical-shift information, and hence deliver improved high-resolution spectroscopic images [30]. Multi-slice implementations using 180° pulses for spatiotemporal encoding and a slice-selective excitation pulse with an arbitrary flip angle, have also been demonstrated [30,31].

In this study, we introduce and explore the performance of SPEN-based strategies for fast spectroscopic imaging of hyperpolarized compounds. Phantom experiments are described to illustrate the feasibility of SPEN-based ^{13}C chemical-shift imaging in such a demanding context. Animal experiments are then presented, monitoring both healthy rats in the region of the kidneys, and mice with EL-4 murine lymphoma tumors as a function of time after injection of hyperpolarized [$1-^{13}\text{C}$]pyruvate. Results are compared against multi-shot CSI sequences with center-out encoding for signal localization, and against a series of 1D spectra, which were used to acquire dynamic information on the progression of pyruvate and lactate labeling. Overall, the results confirm the favorable properties of single-shot spatiotemporal encoding for hyperpolarized ^{13}C imaging *in vivo*. Possible extensions of these experiments are discussed.

2. Theoretical background

2.1. SPEN's simultaneous spatial and spectral encoding

Spatiotemporal encoding relies on a manipulation involving the combined action of a frequency-swept pulse applied in the presence of an encoding gradient, followed by a sequential unraveling of the encoded imaging information using an acquisition gradient [20]. These manipulations can deliver an MR image without the use of a Fourier Transform (FT); when the encoding pulse duration is different from the acquisition duration and/or if no refocusing pulses are used, a built-in spectral encoding is also obtained [27]. This capability to extract both spatial and spectral information from the same Free Induction Decay (FID) can be understood from an analysis of the results arising in a model 1D experiment that uses a chirp pulse for either excitation (Fig. 1a) or inversion

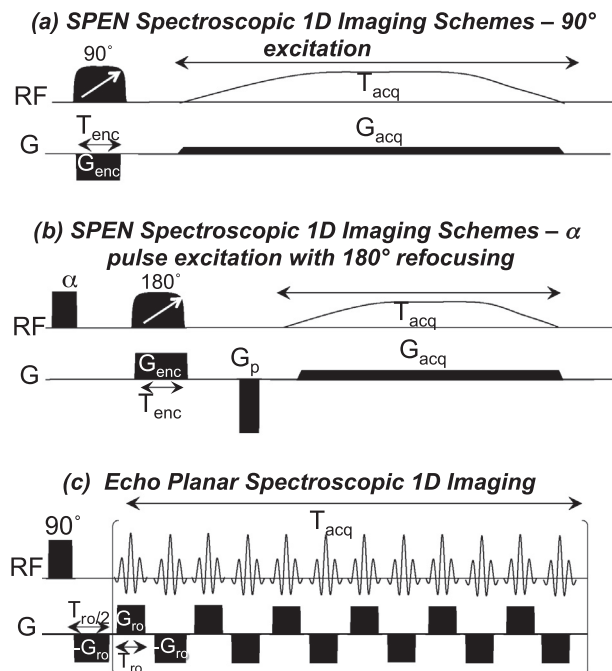


Fig. 1. (a and b) SPEN spectroscopic 1D MRSI schemes based on excitation or refocusing chirp pulses. (c) Echo Planar Spectroscopic 1D imaging.

(Fig. 1b). Assuming that the ensuing FID arises from Q contributing chemical sites $\{w_{cs}^q\}_{q=1..Q}$ spanning a field-of-view FOV being addressed by the swept pulses, its expression can be written as [27]:

$$S(t) = \int_{-\frac{\text{FOV}}{2}}^{\frac{\text{FOV}}{2}} \sum_{q=1}^Q \rho^q(y) e^{i\varphi_{enc}(y, w_{cs}^q)} e^{i(k(t)y + w_{cs}^q t)} dy \quad (1)$$

where $\varphi_{enc}(y, w_{cs}^q) = \alpha_{enc} y^2 + \beta_{enc} y + \text{const}$ and $\{\alpha_{enc} \cdot \beta_{enc}\}_{enc=90^\circ, 180^\circ}$ are coefficients depending on the magnitude and the duration of the encoding gradient (G_{enc} , T_{enc}), as well as on the requested FOV: for the 90° chirp pulse case in Fig. 1a $\alpha_{90^\circ} = -\frac{\gamma G_{enc} T_{enc}}{2 \text{FOV}}$, $\beta_{90^\circ} = \frac{\gamma G_{enc} T_{enc}}{2} - \frac{w_{cs}^q T_{enc}}{\text{FOV}}$; for the 180° adiabatic sweep case in Fig. 1b $\alpha_{180^\circ} = -\frac{\gamma G_{enc} T_{enc}}{2 \text{FOV}}$, $\beta_{180^\circ} = \gamma G_{enc} T_{enc} - \frac{w_{cs}^q T_{enc}}{\text{FOV}}$ with β_{180° including a pre-phasing gradient. The $k(t) = \gamma \int_0^t G_{acq}(t') dt'$ appearing in Eq. (1) is a wavenumber accrued during the acquisition time t , which over the course of its duration T_{acq} should fulfill an action $k_{acq} = G_{enc} \cdot T_{enc}$ in the case of a 90° chirp pulse and $k_{acq} = 2 \cdot G_{enc} \cdot T_{enc}$ in the case of a 180° chirp pulse. Spectral information is contained in the w_{cs}^q -dependent phase terms appearing both in β_{enc} and during the acquisition's time-dependence of Eq. (1). Once represented in a discrete $\rho^q(y_k)$ form, one can describe the signal $S(t)$ by a set of linear equations:

$$\left\{ S(t_i) = \sum_{q=1}^Q S_q(t_i) = \sum_{q=1}^Q \left\{ \sum_{k=1}^M A(t_i, y_k, w_{cs}^q) \rho^q(y_k) \right\} \right\}_{i=1..N} \quad (2)$$

where the $A(t_i, y_k, w_{cs}^q)$ matrix derives from Eq. (1) and contains contributions in its phase arising from SPEN's excitation and acquisition terms, as well as phase contributions due to the chemical shift evolutions. In Eq. (2) N represents the number of acquired points, and M is the number of points desired along the spatial dimension. To solve these equations, all SPEN and chemical shift terms are collected into an extended A_{ext} matrix; the final characterization of the spatial density profile for each chemical site q can then be cast as $S = A_{ext} \rho_{ext}$, where $\rho_{ext}(y_k) = [\rho^1(y_k) \dots \rho^Q(y_k)]$. The spin density y -profile for each chemical site q , $\rho^q(y_k)$, can then be reconstructed by solving an inverse problem using a number of possible minimization methods. The actual method used in this study

for reconstructing spectroscopic images from SPEN experiments is based on the extended Super-Resolution algorithm described in more detail in Ref. [30]. It follows that the spin density 1D image of several chemical sites can be obtained simultaneously in this way using a constant acquisition gradient, with no need for the fast and strong oscillating gradients usually required in the classic EPSI sequence (Fig. 1c).

This 1D spatial/1D spectral scheme can be extended to a single-shot 2D spatial/1D spectral sequence; for instance by encoding the readout dimension in a usual k -space fashion, and retaining the spatiotemporal procedure just described for encoding the low-bandwidth spatial/spectral dimensions. An echo-planar trajectory with appropriate gradients can then be used to explore a hybrid k - and SPEN-based 3D MRSI space in a single acquisition. To enable excitation with arbitrary flip angles, multi-slice 3D spatial imaging and the single-shot acquisition of kinetic data, this sequence was implemented here using a 180° adiabatic swept pulse for encoding as shown in Fig. 1b, leading to the overall 1D spectral/2D spatial multi-slice variant displayed in Fig. 2a. Note that this sequence introduces a second inversion pulse after acquisition to restore the longitudinal magnetizations to $+z$, and thereby enable multiple shots from a single hyperpolarized injection.

2.2. Signal-to-noise ratio (SNR) considerations

The SNR available in single-shot SPEN spectroscopic images can be estimated theoretically and compared to that obtained with multi-shot CSI sequences of the kind usually employed in hyperpolarized MRSI (Fig. 2b), using an approach similar to that used in Ref. [32]. Given the similar T_2^* weighting in both sequences and the relatively long T_2 of the samples, T_2^* and T_2 effects can be neglected in

these theoretical signal intensity estimates. The SNR of a 2D spatial/1D spectral CSI sequence can be estimated as:

$$SNR_{CSI} \propto \left(\sum_{n=1}^{N_{pe1} \cdot N_{pe2}} S_n \right) \cdot \frac{\Delta y \cdot \Delta x \sqrt{N_{sum} \cdot N_{freq}}}{\sqrt{N_{pe1} \cdot N_{pe2}} \cdot SW} \quad (3)$$

where S_n is the signal arising from a given resonance for each of the multiple CSI scans, N_{freq} is the number of points acquired in the FID dimension, N_{pe1} and N_{pe2} are the number of points for each phase-encoding dimension, sw is the spectral width, and Δy , Δx are the image pixel dimensions in the scan plane. The N_{sum} introduced in Eq. (3) accounts for the number of points in the frequency domain that need to be co-added in order to reconstruct an optimal image for a specific chemical peak. Indeed, unlike the case in a high-resolution scenario where this parameter would be unity, a range of points usually has to be co-added in this kind of experiment to reconstruct each site's optimal image; this reflects unavoidable B_0 inhomogeneities, that broaden the peaks and distribute the spatial data over a range of spectral points. In thermal equilibrium experiments all $\{S_n\}_{n=1 \dots N_{pe1} \cdot N_{pe2}}$ will have similar S_0 intensities, and the SNR becomes

$$SNR_{CSI} \propto \Delta y \cdot \Delta x \frac{\sqrt{N_{sum} \cdot N_{freq} \cdot N_{pe1} \cdot N_{pe2}}}{\sqrt{SW}} \quad (4)$$

The SNR of an image reconstructed from a single-shot SPEN acquisition can be described similarly to the SNR of a single-shot EPI acquisition, with an additional factor that accounts for the sequential chirped excitation and observation of the spins. These spatially-discriminating manipulations endow SPEN with a higher immunity to B_0 inhomogeneity than EPI, but also with a lower intrinsic SNR/pixel. The use of Super-Resolution algorithms for reconstructing the SPEN images can make up for these SNR

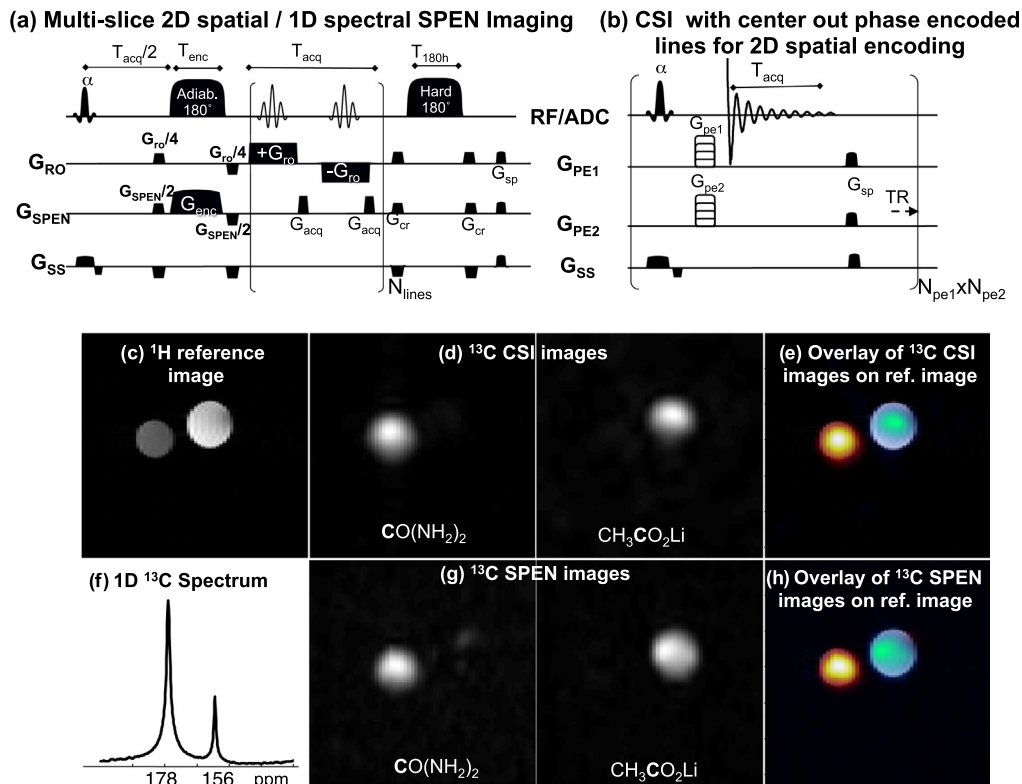


Fig. 2. Comparison of SPEN and CSI results obtained upon ^{13}C chemical shift imaging of a phantom. SPEN and CSI sequences are displayed in (a) and (b), respectively. (c) ^1H reference image of two tubes containing $[1-^{13}\text{C}]$ acetate and $[^{13}\text{C}]$ urea. (f) ^{13}C spectrum of the two tubes. (d and g) Urea and acetate ^{13}C chemical-shift images obtained with CSI and SPEN acquisitions after suitable reconstruction, focusing on the labeled sites indicated in bold. (e and h) ^{13}C chemical-shift images overlaid on the reference ^1H image. See text for further experimental details.

penalties, by summing up multiple contributions to the specific signal that makes up each imaged pixel. These considerations are discussed thoroughly in Ref. [33]; taking them into account it follows that the SNR for a single-shot hybrid SPEN MRSI experiment (Fig. 2a) that incorporates Super-Resolution for the spatial and the spectral reconstruction, can be estimated as:

$$SNR_{SPEN} \propto \Delta y \cdot \Delta x \frac{\sqrt{N_{ro} \cdot N_{SPEN}}}{\sqrt{SW}} \sqrt{\frac{N_{SPEN}/2}{BW \cdot T_{enc}}} \quad (5)$$

where N_{ro} and N_{SPEN} are the number of points acquired in the read-out and SPEN dimensions, and $BW \cdot T_{enc}$ is the time-bandwidth product of the chirp pulse. SNR_{SPEN} must be multiplied by $\sqrt{N_{rep}}$ if its results are averaged over N_{rep} repetitions.

Analyses of these expressions reveal that both approaches should yield comparable SNR's if performed under optimized thermal equilibrium conditions. In hyperpolarized experiments, however, the SNR ratio between multi- and single-shot spectroscopic imaging sequences should shift in favor of the single-scan acquisition if constant flip angle excitations are used, and become comparable if variable flip angle excitation schemes are incorporated in the multi-shot acquisition. The lower performance of the constant-flip-angle acquisitions reflects the drop in the original signal during consecutive CSI shots, which behaves as $S_n \propto \sin(\theta) \cdot (\cos(\theta))^n \cdot e^{-nTR/T_1}$, where $n = 1, \dots, N_{pe1} \cdot N_{pe2}$ is the excitation step in the 2D phase encoding repetitions, θ is the (presumed constant) excitation flip angle, TR is the repetition time and T_1 is the longitudinal relaxation time. Moreover, even if similar SNRs can be obtained, a single shot of the order of 100 ms can provide the full spectral and spatial information of interest, in contrast to the many seconds that are required to obtain the spatial information in CSI or EPSI sequences – and therefore could still prove to have practical advantages from a dynamics standpoint.

3. Materials and methods

3.1. ^{13}C phantom thermal equilibrium experiments

Thermal equilibrium experiments were conducted on a ^{13}C phantom consisting of two tubes, containing [^{13}C]urea and lithium [^{13}C]acetate, providing a chemical shift range of ~ 1500 Hz. The aim of these experiments was to assess signal localization and to validate theoretical SNR estimates for the single- and multi-shot ^{13}C imaging variants. These data were acquired on a 7 T Varian pre-clinical, horizontal-bore scanner (Palo Alto, CA) using a 20 mm $^1\text{H}/^{13}\text{C}$ surface coil. The single-shot hybrid SPEN sequence was compared to a reference multi-shot CSI sequence with a FOV of $4 \times 4 \text{ cm}^2$ and a slice thickness of 1 cm. SPEN acquisitions used the sequence in Fig. 2a, with a 90° initial excitation pulse, $sw = 50 \text{ kHz}$, $T_{enc} = 5 \text{ ms}$, $G_{enc} = 3.8 \text{ G/cm}$, $T_{acq} = 46 \text{ ms}$, $TE = 33..79 \text{ ms}$ (depending on the spins' positions), 16×96 acquired data points (effective resolution of $2.5 \times 0.8 \text{ mm}^2$), $TR = 200 \text{ s}$, and 8 scans leading to a total experiment time of 0.5 h. The CSI parameters were 90° flip angle pulses, $sw = 6 \text{ kHz}$, $T_{acq} = 85 \text{ ms}$, $N_{freq} = 512$, $N_{pe1} \times N_{pe2} = 16 \times 16$ (effective resolution of $2.5 \times 2.5 \text{ mm}^2$), $TR = 60 \text{ s}$ and $\approx 4.3 \text{ h}$ total scan duration. In these SNR comparisons, the measured signal was calculated by drawing a region of interest centered on each tube, while the noise was calculated as the standard deviation in a signal-free region.

3.2. Hyperpolarized ^{13}C experiments on phantoms

These basic SNR tests were followed by hyperpolarized experiments *in vitro*, where DNP-enhanced [^{13}C]pyruvate was injected into a tube and a series of SPEN experiments were performed with various flip angles, to confirm that the signal decayed as expected

given the known T_1 value and repetition time. These experiments were performed on a 4.7 T MRI horizontal-bore magnet (Oxford Instruments, Oxford, UK) interfaced to a Varian scanner and equipped with a dual tuned $^1\text{H}/^{13}\text{C}$ linear volume transmit coil (Rapid Biomedical, Würzburg, Germany) for ^{13}C excitation and with a ^{13}C surface coil for acquisition. Hyperpolarization was carried out with a HyperSense polarizer (Oxford Instruments Molecular Biotech, Tubney Woods, UK). SPEN MRSI data were collected with the sequence shown in Fig. 2a and the following parameters: $\sim 15^\circ$ and $\sim 60^\circ$ excitation angles α , $sw = 31 \text{ kHz}$, $T_{enc} = 8 \text{ ms}$, $G_{enc} = 0.6 \text{ G/cm}$, $T_{acq} = 51 \text{ ms}$, $TE = 39..90 \text{ ms}$, 20×64 acquired data points (effective resolution of $5 \times 3.1 \text{ mm}^2$), FOV of $10 \times 10 \text{ cm}^2$, slice thickness of 1 cm, single scan acquisition of $\approx 90 \text{ ms}$, TR of 1.1 s, and $N_{rep} = 61$ and 11, corresponding to each of the flip angles listed above.

3.3. Hyperpolarized [^{13}C]pyruvate experiments in healthy rats

Hyperpolarized [^{13}C]pyruvate was injected into healthy rats, and a region containing the animals' kidneys was scanned. These experiments focused on the ability of single-shot SPEN to resolve the spectroscopic images of the four peaks – pyruvate, lactate, alanine and bicarbonate – expected to arise due to metabolism. These images were compared against results acquired using a CSI with center-out phase encoding for the two spatial dimensions. The magnet and transmit coil setup in these experiments were the same as in the hyperpolarized phantom experiments, except that a 4-channel ^{13}C phased-array coil (Rapid Biomedical) was used for data acquisition. The FOV was $6 \times 6 \text{ cm}^2$ and the slice thickness 2 cm. The SPEN parameters were: 90° flip angle α , $sw = 31 \text{ kHz}$, $T_{enc} = 8 \text{ ms}$, $G_{enc} = 1 \text{ G/cm}$, $T_{acq} = 51 \text{ ms}$, $TE = 39..90 \text{ ms}$, 20×64 acquired points (effective resolution of $3 \times 3.75 \text{ mm}^2$) and $\approx 90 \text{ ms}$ total acquisition time. The CSI parameters were 10° flip angle, $sw = 4 \text{ kHz}$, $T_{acq} = 64 \text{ ms}$, $N_{freq} = 256$, $N_{pe1} \times N_{pe2} = 16 \times 16$ (effective resolution of $3.75 \times 3.75 \text{ mm}^2$), $TR = 70 \text{ ms}$ and 16 s total scan duration.

Two male Sprague-Dawley rats (250–300 g) were anesthetized with isoflurane (0.8% isoflurane, 0.25 L/min oxygen, and 0.75 L/min air) and a tail vein catheter was inserted to allow administration of hyperpolarized [^{13}C]pyruvate. In order to improve the comparison every animal was subjected to three injections, each of these followed by a different acquisition: first a SPEN acquisition, then a CSI scan, and finally a SPEN acquisition again. A 20 μL volume of [^{13}C]pyruvic acid (Sigma Aldrich, Munich, Germany) containing 15 mM trityl radical OX063 (Oxford Instruments, Tubney Woods, UK) and 1.5 mM Dotarem (Guerbet, Villepinte, France) were inserted into the polarizer. This sample was polarized for approximately 45 min using 100 mW microwaves at 94.108 GHz. The ^{13}C polarization was monitored by solid state NMR with an average 600 s build-up time constant. The hyperpolarized sample was dissolved in 4 mL of a dissolution medium made of 80 mM Tris, 100 mg/L EDTA, 50 mM NaCl and 80 mM NaOH, yielding 80 mM [^{13}C]pyruvate at physiological pH. A volume of 1 mL was injected into the tail vein over a period of 10 s. The transfer time between dissolution and injection was 10 s on average, and MRS data acquisition was initiated 20 s after the start of injection. These measurements, as well as all associated animal-handling procedures, were performed in accordance with the guidelines for use and care of laboratory animals and were approved by the Danish Inspectorate of Animal Experiments.

3.4. Hyperpolarized [^{13}C]pyruvate experiments in mice bearing an EL-4 murine lymphoma tumor model

A final set of *in vivo* experiments were carried out on tumor-implanted mice with the aims of (i) comparing the spectral

resolutions and the degrees of spatial localization achievable in single-shot SPEN versus multi-scan CSI acquisitions (these data were collected on two different mice), and (ii) comparing the time evolutions of signals collected over 60 s using a train of low flip-angle SPEN MRSI repetitions versus signals collected using simple small flip-angle 1D NMR acquisition. These experiments were performed on a 7 T Varian preclinical scanner, using a dual-tuned $^{13}\text{C}/^1\text{H}$ volume coil for transmit and a 20 mm diameter surface coil for ^{13}C receive (Rapid Biomedical). The FOV was $4 \times 4 \text{ cm}^2$ and the slice thickness 1 cm. The SPEN parameters were: 20° flip angle, $sw = 31 \text{ kHz}$, $T_{\text{enc}} = 3 \text{ ms}$, $G_{\text{enc}} = 2.4 \text{ G/cm}$, $T_{\text{acq}} = 41 \text{ ms}$, $TE = 29 \dots 70 \text{ ms}$, 16×64 acquired points (effective resolution of $2.5 \times 1.25 \text{ mm}^2$), single scan acquisition of $\approx 70 \text{ ms}$, $TR = 2.1 \text{ s}$; for an $\approx 60 \text{ s}$ time-progression $N_{\text{rep}} = 30$. The CSI parameters were 5° flip angles α , $sw = 6 \text{ kHz}$, $T_{\text{acq}} = 21 \text{ ms}$, $N_{\text{freq}} = 128$, $N_{\text{pe1}} \times N_{\text{pe2}} = 32 \times 32$ (effective resolution of $1.25 \times 1.25 \text{ mm}^2$), $TR = 30 \text{ ms}$ and 31 s total duration for the 1D spectral/2D spatial scan. For the 1D spectral acquisition scan parameters were: 20° flip angle α , $sw = 6 \text{ kHz}$, $T_{\text{acq}} = 170 \text{ ms}$, $N_{\text{freq}} = 1024$, $TR = 2 \text{ s}$ and $N_{\text{rep}} = 30$.

Experiments were performed on an EL-4 murine lymphoma model. EL-4 cells were grown to a density of ca. 5×10^7 cells/mL in RPMI 1640 medium supplemented with 10% (v/v) fetal-calf serum and 2 mM glutamine. C57/Blk6 female mice (10 weeks old) were injected subcutaneously with 100 μL of a suspension of 5×10^6 EL4 cells in the right flank and tumors were allowed to grow for 9 days ($\sim 2 \text{ cm}^3$ in volume). Prior to the imaging experiments, animals were anaesthetized by administration of a mixture containing O_2 in medical air (25%/75% v/v at 2 L/min) plus 3% isoflurane (Isoflo, Abbotts Laboratories Ltd.) and subsequently 1–2% isoflurane in O_2 /medical air. They were then placed in a dual-tuned $^{13}\text{C}/^1\text{H}$ volume transmit coil, the ^{13}C receive only surface coil was placed immediately over the tumor so that it detected signal that was principally from the latter. A cannula was inserted into the tail vein and its patency maintained through the use of heparin diluted in sterile saline (100 U/mL). 0.2 mL of hyperpolarized $[1-^{13}\text{C}]\text{pyruvate}$ solution ($\sim 80 \text{ mM}$) were injected intravenously into the mouse. A maximum of three injections were given to each mouse. The above experiments were performed under the Animals (Scientific Procedures) Act of 1986 and were approved by local Cambridge University ethical review committees.

3.5. Pulse sequences and processing

For all SPEN experiments, radiofrequency pulses and gradient shapes were designed in Matlab® (The MathWorks Inc., Natick, MA) and uploaded onto the scanners. The reconstruction of SPEN and CSI images and spectra was performed in all instances using custom-written MATLAB packages, which included the possibility to process the SPEN- k -space data with super-resolution along the spatiotemporal dimension and with FT along the k -dimension. Pre-SR data manipulations included minor realignments of positive and negative readout echoes and zero-filling to a 128×128 matrix size.

4. Results and discussion

4.1. ^{13}C phantom experiments

While dissolution-DNP provides an unprecedented increase in NMR signal, applications to molecular imaging are still constrained by the available signal-to-noise ratio. Any increase in acquisition speed must then come with a well understood, and ideally minor, cost in SNR. In order to examine the SNR losses in single-shot SPEN MRSI, and to validate experimental SNR measurements with theoretical estimates, a ^{13}C phantom with two distinct NMR peaks –

^{13}C -labeled urea and $^{13}\text{C}_1$ -acetate in separate tubes – was examined. Fig. 2d–g shows a comparison between chemical-shift images acquired in a single shot with a hybrid SPEN sequence, and reference images obtained with a multi-shot CSI sequence that used 2D phase encoding for the spatial dimensions. While other sequences provide shorter acquisition times [11,12], CSI was selected here to provide a robust reference against which the SNR of single-shot SPEN could be compared. The SPEN images resolved for each of the ^{13}C spectral peaks (Fig. 2), have good spectral definition vis-à-vis the CSI multi-scan counterparts. The SNR ratio between the two images produced by the different methods can be estimated from the scan parameters and compared to the measured SNR ratio, averaged over the acetate and urea peaks. Since the CSI raw data is three dimensional, including two spatial dimensions and a spectral one, the images of chemical sites were reconstructed and integrated over the relevant frequency range for each peak. In our example signals were summed for each peak over a range of $\sim 300 \text{ Hz}$ ($N_{\text{sum}} = 27$) around the peak maximum, to cover most of the resonance while avoiding signal contamination. N_{sum} and other relevant scan parameters from the SNR Eqs. (3)–(5) for CSI and SPEN sequences were considered in the SNR estimation. The calculated $\text{SNR}_{\text{CSI}}/\text{SNR}_{\text{SPEN}}$ for equal pixel size should be ~ 13 for the selected scan parameters (which included many more scans in the CSI acquisitions), while the average $\text{SNR}_{\text{CSI}}/\text{SNR}_{\text{SPEN}}$ measured per pixel was 9. These two values are comparable and within the errors expected from the various assumptions involved in the theoretical estimates. Possible sources for the small discrepancy between the calculated and measured SNRs could lie in our assumption that in CSI different frequency points contribute equally to the signal, or from the fact that longitudinal magnetization may not have been fully restored for the chosen TR . Notice that the CSI experiment took 4.3 h to obtain a resolution of $2.5 \times 2.5 \text{ mm}^2$ (16×16 repetitions with a TR of 60 s), while the SPEN experiment required only a single shot of 80 ms to obtain a resolution of $2.5 \times 0.8 \text{ mm}^2$ and 0.5 h for 8 repetitions with a TR of 200 s. Although, the TR 's in these experiments were different and not entirely optimized, the results serve well the goal of the verification test and reveal the expected SNR and its improvement per unit time. Overall, these results confirm the successful implementation of single-shot SPEN imaging and a good understanding of the relative sensitivities of the two sequences.

Fig. 3 shows the results obtained immediately following the injection of hyperpolarized $[1-^{13}\text{C}]\text{pyruvate}$ into a tube, using a series of single-shot SPEN sequences. The figure shows the results obtained with two different excitation flip angles. The estimated T_1 from the measured signal decay in both experiments was in the range of ~ 40 – 60 s , which is as expected for such a compound.

4.2. Measurements with ^{13}C hyperpolarized pyruvate in rats

In vivo experiments were first performed on healthy rats. Fig. 4 shows spectrally resolved images obtained for pyruvate and for its main metabolic products, lactate, alanine and bicarbonate. The two experiments compared here are single-shot SPEN-based spectroscopic imaging, and a reference multi-shot CSI sequence with a center-out sampling scheme. Overlays of the pyruvate and lactate images on the reference multi-scan ^1H images are also shown. A comparison of the images obtained with SPEN and CSI shows more accurate signal localization for the single-shot technique. Interestingly, small but noticeable differences in signal can be observed between SPEN and CSI, especially for pyruvate. These differences could reflect metabolic fluctuations arising between injections; to further free the method's signal localization from these fluctuations, three injections were performed consecutively on the same animal to acquire images with SPEN, CSI and then again with SPEN. The two SPEN acquisitions showed comparable and consistent

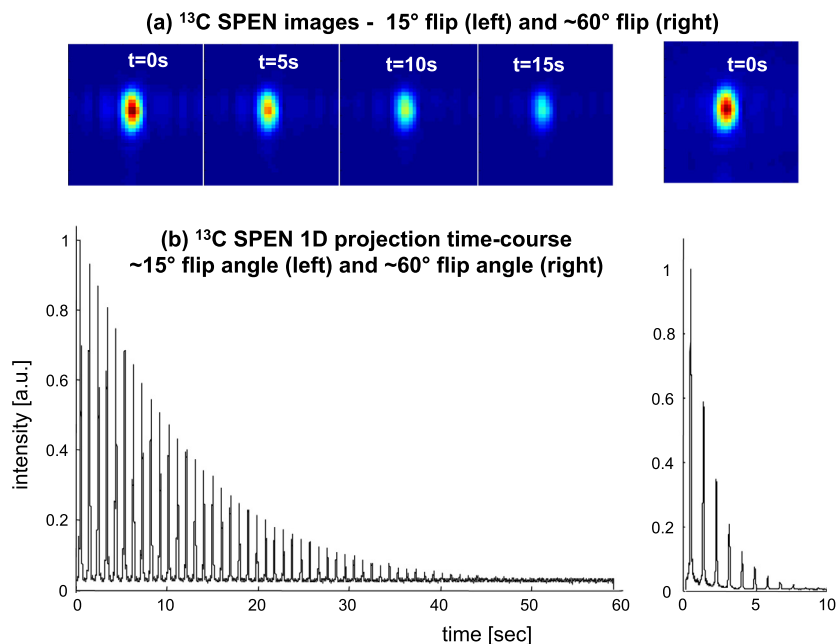


Fig. 3. Measurements of signal decay following injection of hyperpolarized $[1-^{13}\text{C}]$ pyruvate into a tube using SPEN-based spectroscopic imaging. (a) Representative subset of pyruvate images acquired using the Hybrid SPEN sequence in Fig. 2a with flip angles $\alpha \sim 15^\circ$ (left) and $\sim 60^\circ$ (right). (b) 1D profiles from the integrated images as a function of time, for the full train of repetitions.

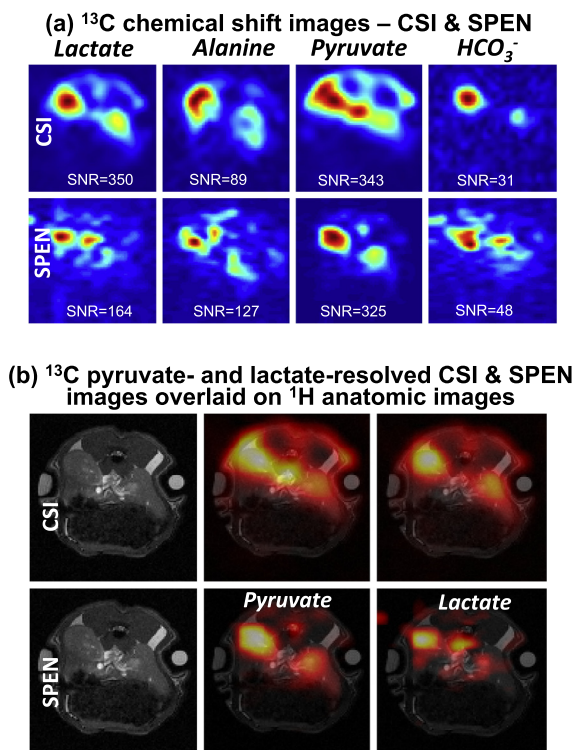


Fig. 4. Representative metabolic images from a rat following injection of hyperpolarized $[1-^{13}\text{C}]$ pyruvate, comparing the results obtained with CSI and single-shot spectrally-resolved experiments. (a) ^{13}C metabolic images obtained with CSI and SPEN for lactate, alanine, pyruvate and bicarbonate (the images are scaled independently – SNR values in the dominant peak regions of each image are displayed). (b) Pyruvate and lactate ^{13}C images overlaid on their corresponding ^1H anatomical images.

SNR, and similar localization results (not shown). An additional source of SPEN/CSI differences could be due the different diffusion weighting that the SPEN sequence, which is based on a spin echo

[34], will incur. Such weighting can decrease significantly the signal from the vasculature, the suppression of which is usually desirable as it can interfere with the measurement of metabolism. Additional differences between the images could arise from the different timescales of the two acquisition modes – with CSI requiring ≈ 16 s for data collection while SPEN only required 90 ms.

Sensitivity considerations are especially relevant for hyperpolarized experiments. The SNR ratio between CSI and SPEN pyruvate images was measured as $\text{SNR}_{\text{CSI}}/\text{SNR}_{\text{SPEN}} \sim 0.95$, while a calculation based on the scan parameters predicted a $\text{SNR}_{\text{CSI}}/\text{SNR}_{\text{SPEN}} \sim 0.6$ – note that the excitation flip angle was 90° for SPEN and 10° for CSI. The difference in the experimental and theoretical SNR ratio is reasonable, considering the variability involved in *in vivo* hyperpolarized injection experiments.

Since the measurement of metabolic rates using hyperpolarized $[1-^{13}\text{C}]$ pyruvate imaging could become an important diagnostic tool in tumor imaging, a set of such experiments was conducted. The performance of single-shot SPEN-based spectroscopic imaging was tested in such a setting, using mice with implanted EL-4 lymphoma tumors. In these experiments, only pyruvate and lactate are present in significant concentrations; therefore only these two metabolites were analyzed. In a first stage we focused again on comparing the signal localization in the pyruvate and lactate images, spectrally-resolved by the single-shot hybrid SPEN sequence, versus images obtained with a CSI sequence (this comparison is shown in two different mice). The resulting images, displayed in Fig. 5a and b, show a reasonable localization of the lactate and pyruvate signals with the SPEN-based sequence. In both cases, SPEN and CSI, the signal follows the tumor shape, as can be appreciated from the ^1H proton reference images. An advantage afforded by single-shot MRSI sequences such as SPEN, is that they can be repeated numerous times after injection of a hyperpolarized substrate. The resulting data set can then be analyzed to obtain a time course for the metabolic conversion of the injected metabolite in pre-selected regions, thereby affording insight into the kinetics of utilization. Fig. 5c shows such a time course, where a train of SPEN repetitions executed with a 20° flip angle were used to obtain a time series of images for pyruvate and lactate; these signals were

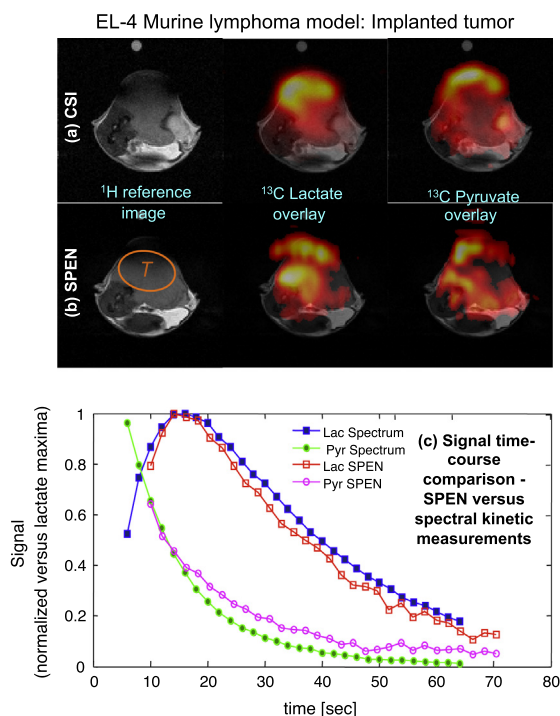


Fig. 5. Representative ^{13}C images acquired after injection of $[1-^{13}\text{C}]$ pyruvate in mice. (a and b) ^1H anatomic images overlaid with ^{13}C images of pyruvate and lactate obtained using CSI and SPEN. The region indicated by “T” marks the approximate tumor location. (c) Comparison of the pyruvate and lactate time courses obtained with SPEN-based spectroscopic imaging and with 1D experiments. The SPEN time-course was obtained by averaging over a region of interest where the signal was most intense (from “T”). A flip angle of 20° and a repetition time of 2 s were used in both experiments.

averaged over the major tumor region shown by the “T” in Fig. 5b. In this tumor a reference time course was also obtained with a series of low-flip-angle 1D spectral acquisitions, localized to a slice through the tumor. Fig. 5c shows good agreement between the time courses obtained with SPEN and with 1D ^{13}C spectral acquisitions. Overall, these results confirm that SPEN-based single-shot spectroscopic imaging methods can yield detailed spatial, spectral and temporal information, similar to that obtained from both multi-shot multidimensional spectroscopic imaging acquisitions and from 1D NMR spectroscopy. This offers new opportunities to investigate metabolic exchange rates in a spatially resolved manner.

5. Conclusions

The first results obtained *in vivo* using single-shot SPEN for chemical-shift imaging in hyperpolarized ^{13}C experiments have been demonstrated. This MRSI approach makes it possible to obtain, within 100 ms, 2D images for several compounds simultaneously. In healthy rats four metabolite peaks were observed; in mice with implanted tumors, a series of images could be obtained for pyruvate and lactate. Images obtained with single-shot SPEN were found to have comparable qualities to those obtained with a CSI sequence, despite the fact that the latter requires orders-of-magnitude longer signal acquisition durations due to the high number of excitation pulses. Although further optimizations could yield improved spectral and spatial resolution as well as added sensitivity, the current results already show that SPEN-based sequences can be utilized as a modality for fast dynamic imaging. Further developments are in progress to exploit additional benefits of spatiotemporal encoding, such as a built-in restricted FOV capa-

bility [24,26], multi-echo experiments and parallel imaging acquisition [35].

Acknowledgments

We are thankful to Sascha Gude, Piotr Dzien and Tiago Rodrigues for laboratory assistance. ERC Advanced Grant #246754, Marie Curie Action ITN Metaflux (Project# 264780), DIP (Project# 710907, Germany), The Danish Kidney Foundation, Helen and Ejnar Bjoernows Foundation, CRUK Programme Grant (C14303/A17197) and the COST Action TD-1103 EuroHyperPol Grant, are gratefully acknowledged for financial support.

References

- [1] J.H. Ardenkjaer-Larsen, B. Fridlund, A. Gram, G. Hansson, L. Hansson, M.H. Lerche, R. Servin, M. Thaning, K. Golman, Increase in signal-to-noise ratio of $>10,000$ times in liquid-state NMR, *Proc. Natl. Acad. Sci. USA* 100 (18) (2003) 10158–10163.
- [2] K. Golman, J.H. Ardenkjaer-Larsen, J.S. Petersson, S. Mansson, I. Leunbach, Molecular imaging with endogenous substances, *Proc. Natl. Acad. Sci. U.S.A.* 100 (18) (2003) 10435–10439.
- [3] A.P. Chen, M.J. Albers, C.H. Cunningham, S.J. Kohler, Y.-F. Yen, R.E. Hurd, J. Tropp, R. Bok, J.M. Pauly, S.J. Nelson, J. Kurhanewicz, D.B. Vigneron, Hyperpolarized C-13 spectroscopic imaging of the TRAMP mouse at 3 T-initial experience, *Magn. Reson. Med.* 58 (6) (2007) 1099–1106.
- [4] A.Z. Lau, A.P. Chen, N.R. Ghugre, V. Ramanan, W.W. Lam, K.A. Connelly, G.A. Wright, C.H. Cunningham, Rapid multislice imaging of hyperpolarized ^{13}C pyruvate and bicarbonate in the heart, *Magn. Reson. Med.* 64 (5) (2010) 1323–1331.
- [5] T.H. Witney, M.I. Kettunen, D.-E. Hu, F.A. Gallagher, S.E. Bohndiek, R. Napolitano, K.M. Brindle, Detecting treatment response in a model of human breast adenocarcinoma using hyperpolarized $[1-^{13}\text{C}]$ pyruvate and $[1,4-^{13}\text{C}_2]$ fumarate, *Br. J. Cancer* 103 (9) (2010) 1400–1406.
- [6] T. Harris, G. Eliyahu, L. Frydman, H. Degani, Kinetics of hyperpolarized ^{13}C pyruvate transport and metabolism in living human breast cancer cells, *Proc. Natl. Acad. Sci. U.S.A.* 106 (43) (2009) 18131–18136.
- [7] C. von Morze, P.E. Larson, S. Hu, K. Keshari, D.M. Wilson, J.-H. Ardenkjaer-Larsen, A. Goga, R. Bok, J. Kurhanewicz, D.B. Vigneron, Imaging of blood flow using hyperpolarized ^{13}C urea in preclinical cancer models, *J. Magn. Reson. Imag.* 33 (3) (2011) 692–697.
- [8] S.A. Butt, L.V. Sogaard, P.O. Magnusson, M.H. Lauritzen, C. Laustsen, P. Åkeson, J.H. Ardenkjaer-Larsen, Imaging cerebral 2-ketoisocaproate metabolism with hyperpolarized ^{13}C magnetic resonance spectroscopic imaging, *J. Cereb. Blood Flow Metab.* 32 (2012) 1508–1514.
- [9] F.A. Gallagher, M.I. Kettunen, S.E. Day, D.E. Hu, J.H. Ardenkjaer-Larsen, R. in ‘t Zandt, P.R. Jensen, M. Karlsson, K. Golman, M.H. Lerch, K.M. Brindle, Magnetic resonance imaging of pH *in vivo* using hyperpolarized ^{13}C -labeled bicarbonate, *Nature* 453 (2008) 940–943.
- [10] S.E. Bohndiek, M.I. Kettunen, D. Hu, B.W.C. Kennedy, J. Boren, F.A. Gallagher, K.M. Brindle, Hyperpolarized $[1-^{13}\text{C}]$ -ascorbic and dehydroascorbic acid: vitamin C as a probe for imaging redox status *in vivo*, *J. Am. Chem. Soc.* 133 (2011) 11795–11801.
- [11] P.E.Z. Larson, R. Bok, A.B. Kerr, M. Lustig, S. Hu, A.P. Chen, S.J. Nelson, J.M. Pauly, J. Kurhanewicz, D.B. Vigneron, Investigation of tumor hyperpolarized $[1-^{13}\text{C}]$ -pyruvate dynamics using time resolved multiband RF excitation echo-planar MRSI, *Magn. Reson. Med.* 63 (3) (2010) 582–591.
- [12] P.E. Larson, S. Hu, M. Lustig, A.B. Kerr, S.J. Nelson, J. Kurhanewicz, J.M. Pauly, D.B. Vigneron, Fast dynamic 3D MR spectroscopic imaging with compressed sensing and multiband excitation pulses for hyperpolarized ^{13}C studies, *Magn. Reson. Med.* 65 (3) (2011) 610–619.
- [13] D. Mayer, Y.F. Yen, J. Tropp, A. Pfefferbaum, R.E. Hurd, D.M. Spielman, Application of subsecond spiral chemical shift imaging to real-time multislice metabolic imaging of the rat *in vivo* after injection of hyperpolarized $[1-^{13}\text{C}]$ pyruvate, *Magn. Reson. Med.* 62 (3) (2009) 557–564.
- [14] S. Hu, M. Lustig, A. Balakrishnan, P.E. Larson, R. Bok, J. Kurhanewicz, S.J. Nelson, A. Goga, J.M. Pauly, D.B. Vigneron, 3D compressed sensing for highly accelerated hyperpolarized ^{13}C MRSI with *in vivo* applications to transgenic mouse models of cancer, *Magn. Reson. Med.* 63 (2) (2010) 312–321.
- [15] Y.S. Levin, D. Mayer, Y.-F. Yen, R.E. Hurd, D.M. Spielman, Optimization of fast spiral chemical shift imaging using least squares reconstruction: application for hyperpolarized ^{13}C metabolic imaging, *Magn. Reson. Med.* 58 (2007) 245–252.
- [16] J.W. Gordon, D.J. Niles, S.B. Fain, K.M. Johnson, Joint spatial-spectral reconstruction and k-t spirals for accelerated 2D spatial/1D spectral imaging of ^{13}C dynamics, *Magn. Reson. Med.* (2013), <http://dx.doi.org/10.1002/mrm.24796>.
- [17] C.H. Cunningham, D.B. Vigneron, A.P. Chen, D. Xu, S.J. Nelson, R.E. Hurd, D. Kelley, J.M. Pauly, Design of flyback echo-planar readout gradients for magnetic resonance spectroscopic imaging, *Magn. Reson. Med.* 54 (2005) 1286–1289.

- [18] G.D. Reed, P.Z. Larson, C. von Morze, R. Bok, M. Lustig, A.B. Kerr, J.M. Pauly, J. Kurhanewicz, D.B. Vigneron, A method for simultaneous echo planar imaging of hyperpolarized ^{13}C pyruvate and ^{13}C lactate, *J. Magn. Reson.* 217 (2012) 41–47.
- [19] L. Frydman, T. Scherf, A. Lupulescu, The acquisition of multidimensional NMR spectra within a single scan, *Proc. Natl. Acad. Sci.* 99 (25) (2002) 15858.
- [20] A. Tal, L. Frydman, Single-scan multidimensional magnetic resonance, *Prog. Nucl. Magn. Reson. Spectrosc.* 57 (2010) 241–292.
- [21] D. Kunz, Use of frequency-modulated radiofrequency pulses in MR imaging experiments, *Magn. Reson. Med.* 3 (1986) 377–384.
- [22] J.G. Pipe, Spatial encoding and reconstruction in MRI with quadratic phase profiles, *Magn. Reson. Med.* 33 (1995) 24–33.
- [23] Y. Shrot, L. Frydman, Spatially-encoded NMR and the acquisition of 2D magnetic resonance images within a single scan, *J. Magn. Reson.* 172 (2005) 179–190.
- [24] R. Chamberlain, J.Y. Park, C. Corum, E. Yacoub, K. Ugurbil, C.R. Jack, M. Garwood, RASER: a new ultrafast magnetic resonance imaging method, *Magn. Reson. Med.* 58 (4) (2007) 794–799.
- [25] N. Ben-Eliezer, Y. Shrot, L. Frydman, High-definition single-scan 2D MRI in inhomogeneous fields using spatial encoding methods, *Magn. Reson. Imag.* 28 (1) (2010) 77–86.
- [26] R. Schmidt, L. Frydman, New spatiotemporal approaches for fully refocused, multislice ultrafast 2D MRI, *Magn. Reson. Med.* (2014), <http://dx.doi.org/10.1002/mrm.24714>.
- [27] A. Tal, L. Frydman, Spectroscopic imaging from spatially-encoded single-scan multidimensional MRI data, *J. Magn. Reson.* 189 (2007) 46–58.
- [28] N. Ben-Eliezer, M. Irani, L. Frydman, Super-resolved spatially-encoded single-scan 2D MRI, *Magn. Reson. Med.* 63 (6) (2010) 1594–1600.
- [29] C. Cai, J. Dong, S. Cai, J. Li, Y. Chen, L. Bao, Z. Chen, An efficient de-convolution reconstruction method for spatiotemporal-encoding single-scan 2D MRI, *J. Magn. Reson.* 228 (2013) 136–147.
- [30] R. Schmidt, L. Frydman, In vivo 3D spatial/1D spectral imaging by spatiotemporal encoding: a new single-shot experimental and processing approach, *Magn. Reson. Med.* 70 (2013) 382–391.
- [31] N. Ben-Eliezer, L. Frydman, Spatiotemporal encoding as a robust basis for fast three-dimensional in vivo MRI, *NMR Biomed.* 24 (2011) 1191–1201.
- [32] R. Pohmann, M. Kienlin, A. Haase, Theoretical evaluation and comparison of fast chemical shift imaging methods, *J. Magn. Reson.* 129 (1997) 145–160.
- [33] N. Ben-Eliezer, Y. Shrot, L. Frydman, D.K. Sodickson, Parametric analysis of the spatial resolution and signal-to-noise ratio in super-resolved spatiotemporally encoded (SPEN) MRI, *Magn. Reson. Med.* (2014), <http://dx.doi.org/10.1002/mrm.24954>.
- [34] M.I. Kettunen, B.W.C. Kennedy, D. Hu, K.M. Brindle, Spin echo measurements of the extravasation and tumor cell uptake of hyperpolarized $[1-^{13}\text{C}]$ lactate and $[1-^{13}\text{C}]$ pyruvate, *Magn. Reson. Med.* 70 (2013) 1200–1209.
- [35] R. Schmidt, B. Baishya, N. Ben-Eliezer, A. Seginer, L. Frydman, Super-resolved parallel MRI by spatiotemporal encoding, *Magn. Reson. Imag.* 32 (2014) 60–70.